

# *In vivo* reflectance confocal microscopy of shave biopsy wounds: feasibility of intraoperative mapping of cancer margins

A. Scope, U. Mahmood, D.S. Gareau, M. Kenkre, J.A. Lieb, K.S. Nehal and M. Rajadhyaksha

Dermatology Service, Memorial Sloan-Kettering Cancer Center, New York, NY, U.S.A.

## Summary

### Correspondence

Alon Scope.

E-mail: scopea1@gmail.com

### Accepted for publication

6 September 2010

### Funding sources

This research was funded in part by the National Institutes of Health (NIH) grant R44 CA093106 from the National Cancer Institute, NIH grant R01EB002715 from the Image-Guided Interventions program of the National Institute of Biomedical Imaging and Bioengineering and a grant from the Byrne Fund, Department of Medicine at Memorial Sloan-Kettering Cancer Center.

### Conflicts of interest

M.R. is a former employee and owns equity in Lucid Inc., the company that makes and sells the VivaScope confocal microscope. The VivaScope is the commercial version of an original laboratory prototype of a confocal scanning laser microscope that was developed by M.R. when he was in the Department of Dermatology at Massachusetts General Hospital, Harvard Medical School. All other authors have no conflicts of interest to declare.

DOI 10.1111/j.1365-2133.2010.10063.x

Over two million individuals are treated annually for non-melanoma skin cancers (NMSCs) in the U.S.A. with costs exceeding 1 billion dollars.<sup>1,2</sup> As NMSCs often develop on the face, Mohs micrographic surgery (MMS) is used as tissue-preserving technique. During MMS, tumour is excised with narrow margins and the surgeon assesses margins on frozen histopathological sections; any residual tumour is mapped and corresponding tissue is further excised. Processing frozen sections takes 20–45 min per stage of MMS. An intraoperative imaging modality which permits direct detection of residual tumour in surgical wounds may potentially expedite MMS.

**Background** Reflectance confocal microscopy (RCM) images skin at cellular resolution and has shown utility for the diagnosis of nonmelanoma skin cancer *in vivo*. Topical application of aluminium chloride (AlCl<sub>3</sub>) enhances contrast in RCM images by brightening nuclei.

**Objectives** To investigate feasibility of RCM imaging of shave biopsy wounds using AlCl<sub>3</sub> as a contrast agent.

**Methods** AlCl<sub>3</sub> staining was optimized, in terms of concentration vs. immersion time, on excised tissue *ex vivo*. RCM imaging protocol was tested in patients undergoing shave biopsies. The RCM images were retrospectively analysed and compared with the corresponding histopathology.

**Results** For 35% AlCl<sub>3</sub>, routinely used for haemostasis in clinic, minimum immersion time was determined to be 1 min. We identified three consistent patterns of margins on RCM mosaic images by varying depth: epidermal margins, peripheral dermal margins, and deep dermal margins. Tumour islands of basal cell carcinoma were identified at peripheral or deep dermal margins, correlating on histopathology with aggregates of neoplastic basaloid cells. Atypical cobblestone or honeycomb patterns were identified at the epidermal margins in squamous cell carcinomas, correlating with a proliferation of atypical keratinocytes extending to biopsy margins.

**Conclusions** RCM imaging of shave biopsy wounds is feasible and demonstrates the future possibility of intraoperative mapping in surgical wounds.

To this end, reflectance confocal microscopy (RCM), a noninvasive imaging technique with cellular-level resolution,<sup>3,4</sup> has shown promise for diagnosis of NMSC. RCM was found to have sensitivity of 92% and specificity of 97% for presurgical *in vivo* diagnosis of basal cell carcinoma (BCC).<sup>5</sup> Tannous *et al.*<sup>6</sup> demonstrated in a small case series the potential of intraoperative RCM to guide MMS; the investigators also found that aluminium chloride (AlCl<sub>3</sub>), routinely used for haemostasis during skin surgery, enhances contrast between aggregates of BCC and surrounding dermis in RCM images. Recent work also demonstrated the feasibility of *ex vivo* mosaicing confocal microscopy to enable rapid detec-

tion of BCCs in skin excision specimens from MMS, using exogenous fluorescent contrast agents to stain nuclear morphology.<sup>7–9</sup> However, use of fluorescent contrast agents for *in vivo* imaging is still being tested for efficacy and toxicity<sup>10,11</sup> and this method is not yet ready for clinical use. Thus, reflectance-based RCM imaging continues to advance more rapidly towards clinical applications.<sup>12–16</sup> Other optical technologies have been used for preoperative detection of margins of BCC. Reported studies included the use of dermoscopy,<sup>17</sup> fluorescence imaging using Wood's lamp excitation and 5-aminolaevulinic acid-induced protoporphyrin IX,<sup>18–20</sup> ultrasound imaging,<sup>21,22</sup> optical coherence tomography<sup>23</sup> and Raman microspectroscopy.<sup>24,25</sup> However, to the best of our knowledge, none has yet been applied for imaging wounds with contrast agents or under intraoperative conditions in human skin.

Building upon the initial observations of Tannous *et al.*,<sup>6</sup> we performed a prospective study, to investigate more rigorously the feasibility of RCM for intraoperative assessment of tumour margins in a larger series of surgical wounds. First, the utility of AlCl<sub>3</sub> was further investigated on excised tissue. Next, we imaged shave biopsy wounds as a model for initial stages of MMS. Mosaicing, a recent advance in RCM imaging,<sup>26–28</sup> was used; mosaicing allows observation of larger fields-of-view of surgical wound margins, akin to low-magnification histopathology. Establishing imaging protocols and identifying current imaging performance and challenges are necessary translational steps, towards the long-term goal of developing RCM as a guide to surgery.

## Materials and methods

### Preclinical study of aluminium chloride as contrast stain

Freshly excised specimens were obtained from MMS performed at Memorial Sloan-Kettering Cancer Center (MSKCC). During MMS, excised specimens are frozen and haematoxylin and eosin (H&E)-stained sections are prepared and examined. Remaining tissue, which is routinely discarded, was collected for this study, under Institutional Review Board approval.

Each specimen was thawed, rinsed in normal saline and imaged *ex vivo* using a previously described bench-top reflectance confocal microscope (VivaScope 2500; Lucid Inc., Rochester, NY, U.S.A.).<sup>26,28</sup> Subsequently, specimens were rinsed with saline, immersed in AlCl<sub>3</sub> and re-imaged. Concentrations of AlCl<sub>3</sub> and immersion times were varied to determine optimal imaging conditions. Concentrations tested were 20% in anhydrous ethyl alcohol, 35% in purified water, 50% in purified water and 50% in equal volumes of isopropanol and purified water. Immersion times were 5, 10, 30 and 45 s and 1, 2, 3 and 5 min. Minimum immersion time was defined as time required for all nuclei in the RCM mosaic to appear consistently brightened. Each condition was retested on a minimum of five specimens.

## Reflectance confocal microscopy imaging study on shave biopsy wounds

### Patients

Participants were recruited from patients undergoing shave biopsy for diagnosis of suspicious skin lesions at MSKCC. All patients were 18 years or older. Written consent was obtained prior to enrolment. The research protocol was approved by MSKCC Institutional Review Board.

### Instrumentation

For imaging patients, a commercially available, previously described reflectance confocal microscope (VivaScope 1500; Lucid Inc.) was used.<sup>4,29</sup> Briefly, RCM uses near-infrared laser at 830 nm. A 30 × objective lens allows imaging with optical sectioning of 3 µm and lateral resolution of 1 µm. Contact between the objective lens and skin is achieved with a tissue ring. The reflectance confocal microscope acquires images of *en face* optical sections with 500 × 500 µm field-of-view (equivalent to 30 × magnification). An automated stepper was used to acquire up to 12 × 12 contiguous images into a 'mosaic' which displays a 6 × 6 mm field-of-view (equivalent to 3 × magnification). RCM images can be acquired to a depth of approximately 300 µm.

### Reflectance confocal microscopy imaging protocol

A pilot was conducted during the first eight cases, to assess qualitatively the best imaging conditions and to construct a protocol. For immersion medium in the wound cavity, sterile Surgilube gel (Fougera, Melville, NY, U.S.A.) was used. The gel's viscosity was found to be advantageous compared with sterile saline; the gel was better retained in the wound when imaging patients in recumbent position. Sterile conditions were ensured by draping the wound with transparent dressing (Tegaderm; 3M, St Paul, MN, U.S.A.). Imaging was tested through a 1-mm thick disposable optical window made of polycarbonate disc (General Electric Company, Fairfield, CT, U.S.A.); image quality with the polycarbonate disc was qualitatively better than that obtained with a glass window. Following the results of our preclinical study, we used AlCl<sub>3</sub> solution as a contrast agent in RCM images.

The final protocol was as follows:

- 1 The wound was swabbed with AlCl<sub>3</sub> using sterile applicators.
- 2 The cavity was filled with sterile gel (Fig. 1).
- 3 The wound was sealed with sterile transparent adhesive dressing.
- 4 A drop of Crodamol STS oil (Croda Inc., Edison, NJ, U.S.A.) was applied over the dressing.
- 5 The tissue ring with polycarbonate window was attached to the surface of the dressing. The ring covered part of the wound cavity and part of the wound edge.

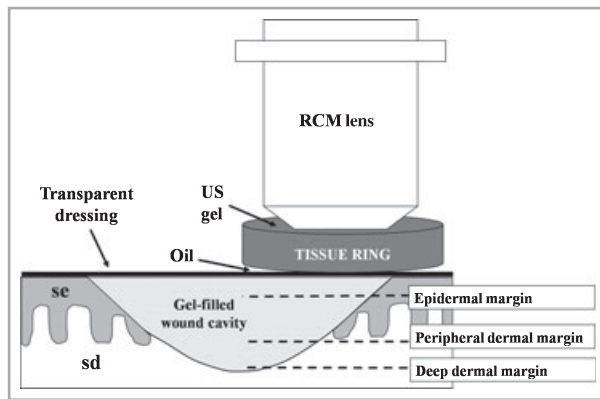


**Fig 1.** Setup for attachment of reflectance confocal microscope (RCM) objective lens to shave biopsy wound. The skin at the site of imaging includes the surgical wound cavity with adjacent intact surrounding epidermis (se) and dermis (sd). The surgical wound cavity is filled with sterile gel and covered by transparent sterile dressing. Following the application of an oil drop on to the dressing, the tissue ring is attached to the dressing, to cover both a portion of the wound cavity and its margins. The top, concave side of the tissue ring is filled with ultrasound (US) gel as the immersion medium. The tissue ring serves as a docking template for the RCM objective lens for locating and stabilizing the site to be imaged. The three depth levels of *en face* reflectance confocal microscopy imaging are shown, including the epidermal margin at the level of the surrounding epidermis, peripheral dermal margin at the level of the surrounding superficial dermis, and deep dermal margin at the level of the base of the wound.

6 Ultrasound gel was used as immersion medium between the tissue ring and the objective lens.

7 RCM images and mosaics were acquired at a minimum of three levels (Fig. 1): level of intact epidermis surrounding the wound ('epidermal margin'), level of superficial dermis in the wound ('peripheral dermal margin') and base of the wound ('deep dermal margin').

Using the final protocol, 39 additional lesions undergoing shave biopsy were included. Histopathological diagnoses for these lesions were BCC ( $n = 10$ ), squamous cell carcinoma (SCC,  $n = 10$ ), actinic keratosis ( $n = 1$ ), irritated seborrhoeic keratosis/lichen planus-like keratosis ( $n = 11$ ), melanoma ( $n = 3$ ), naevus ( $n = 1$ ), irritated verruca ( $n = 2$ ) and neurofibroma ( $n = 1$ ).

### Assessment of reflectance confocal microscopy images and histopathological correlation

Images were jointly assessed by two dermatologists (A.S. and K.S.N.), one of whom (K.S.N.) is an MMS surgeon. Image quality was assessed as acceptable or poor. A mosaic image was considered acceptable if at least 75% of images that show wound margins displayed adequate resolution and contrast as previously defined.<sup>30</sup> For every RCM mosaic, the observers assessed the presence of the following structures: surrounding epidermis; surrounding dermis; bright keratinocytes, bright adnexal epithelium, collagen bundles and inflammatory cells within the wound; and tumour aggregates.

All biopsy specimens were routinely processed with formalin fixation and paraffin embedding, followed by vertical sectioning and H&E staining. Diagnoses were retrieved from the hospital information system. Slides were also examined (by A.S.) for findings which appeared best to correlate with RCM structures under analysis.

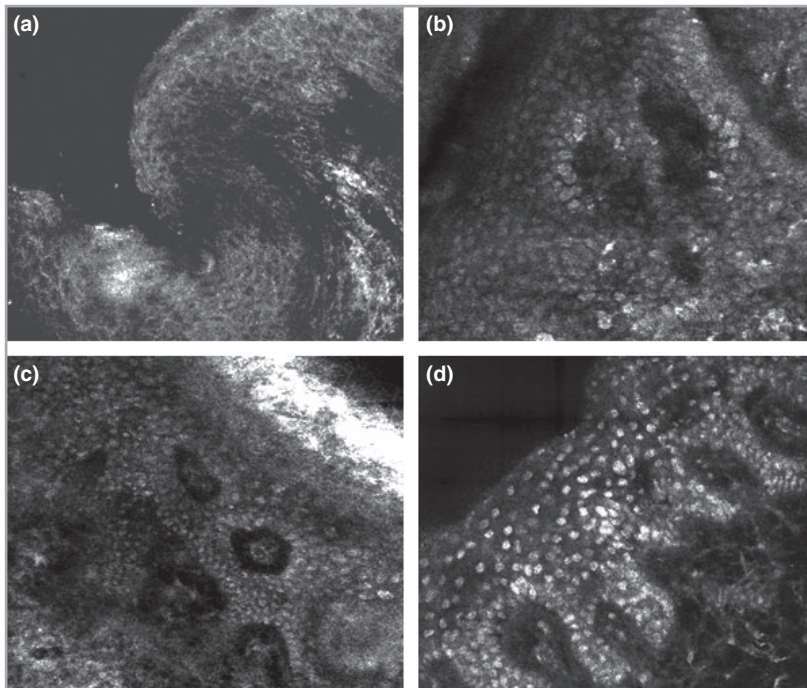


**Fig 2.** Aluminium chloride ( $\text{AlCl}_3$ )-stained epidermis showing nuclear brightening and enhanced nuclei-to-dermis contrast for different immersion times and  $\text{AlCl}_3$  concentrations. The epidermis is vertically sectioned. (a) Unstained control; (b) 20%  $\text{AlCl}_3$ , 3 min of immersion; (c) 35%  $\text{AlCl}_3$ , 1 min of immersion; and (d) 50%  $\text{AlCl}_3$  in water, 10 s of immersion. While the unstained image (a) shows a honeycomb pattern of dark nuclei and bright cellular outlines in the epidermis as normally seen with *in vivo* reflectance confocal microscopy, all  $\text{AlCl}_3$ -stained tissue specimens (b–d) present a cobblestone pattern of bright nuclei in the epidermis (E-epidermis, D-dermis).

**Table 1** Definitions and histopathological correlations of reflectance confocal microscopy (RCM) terms

RCM term	Morphological description	Margin levels; wound tissue vs. surrounding skin	Histopathological correlation
Honeycomb pattern	A pattern whose lines are formed by well-demarcated, polygonal outlines of keratinocytes and whose holes are formed by the dark central nuclei of keratinocytes	Epidermal margins; surrounding epidermis	Normal keratinocytes of spinous and granular layers
Atypical honeycomb pattern	There is an irregular pattern formed by lines that vary in thickness and brightness and holes that vary in size and shape. There are cells that appear wholly bright, without central dark nucleus	Epidermal margins; surrounding epidermis	Atypical keratinocytes with nuclei that are crowded, pleomorphic and hyperchromatic; dyskeratotic keratinocytes; abnormal maturation of epidermis
Cobblestone pattern	Small bright round to oval nuclei of keratinocytes that are uniformly sized and spaced and are separated by less refractile cytoplasm of keratinocytes	Epidermal and peripheral dermal margins; epidermis within the wound	Normal keratinocytes of basal, spinous and granular layers
Atypical cobblestone pattern	Bright nuclei of keratinocytes that are irregularly crowded and display variability in the size of nuclei and the presence of abnormally large nuclei	Can be seen at all margin levels in some cases of SCC; epidermis within wound	Atypical keratinocytes with nuclei that are crowded, pleomorphic and hyperchromatic; dyskeratotic keratinocytes; abnormal maturation of epidermis
Collagen	Very bright discrete fibrillar structures (papillary dermis) or elongated bundles (reticular dermis) with no cellular component and no visible nucleus	Peripheral and deep dermal margins; highly refractile in dermis within wound, blurred and less refractile in surrounding dermis	Collagen of the papillary or reticular dermis
Solar elastosis	Bright, thickened, blurred wavy fibrillar structures with less refractile amorphous background	Peripheral and deep dermal margins; refractile in dermis within wound, blurred and less refractile in surrounding dermis	Solar elastosis in dermis
Bright stellate cells and small bright spots	Larger (> 20 µm), irregularly shaped bright cells and smaller bright round structures (< 20 µm). These cells are usually irregularly spaced (in contrast to cobblestone pattern)	Peripheral and deep dermal margins; refractile in dermis within wound	Lymphocytes and histiocytes

SCC, squamous cell carcinoma.

## Results

### Preclinical study of aluminium chloride as contrast stain

RCM imaging of normal epidermis from excised tissue is shown (Fig. 2). Under unstained conditions, nuclei of keratinocytes appear dark and cytoplasm and intercellular borders between keratinocytes appear as bright polygonal outlines resulting in a honeycomb pattern at spinous and granular layers of the epidermis (Fig. 2a and Table 1). After immersion in AlCl<sub>3</sub>, nuclei of keratinocytes appear bright (Fig. 2b–d) with enhanced nuclear-to-cytoplasm contrast, resulting in a cobblestone pattern (Table 1). The minimum immersion time for various AlCl<sub>3</sub> concentrations is also shown (Table 2).

**Table 2** The minimum immersion time vs. concentration of aluminium chloride to attain consistent nuclear brightening

Concentration of aluminium chloride	Minimum time (s)
20%	180
35%	60
50% in isopropanol + water	10
50% in purified water	10

The results of the preclinical study were empirically translated to the protocol for imaging shave biopsy wounds in patients. The routinely used concentration of AlCl<sub>3</sub> in our clinic is 35% for which the minimum immersion time was determined to be 1 min (Fig. 2c). This was translated to

swabbing the wound with  $\text{AlCl}_3$  four times with a sterile applicator (each swab was used for about 15 s), resulting in an immersion time of 1 min.

### Reflectance confocal microscopy imaging study on shave biopsy wounds

#### Correlation of confocal and histopathological features of normal skin

Using the final protocol, 39 lesions undergoing shave biopsy were imaged with RCM and analysed. Bright nuclei of keratinocytes within the wound cavity were seen in 21 lesions (54%). These bright nuclei were uniformly spaced, forming a regular cobblestone pattern (Table 1, Fig. 3a). As the epidermis overlying the surgical wound lacks a stratum corneum, the keratinocytes within the wound cavity were exposed to  $\text{AlCl}_3$  application. In contrast, the epidermis of the surrounding skin showed a honeycomb pattern (Table 1, Fig. 3b), similar to the appearance of unstained epidermis in the preclinical study and similar to *in vivo* imaging of epidermis of normal skin.<sup>21</sup> The regular cobblestone and honeycomb patterns correlate with normal patterns of keratinocytes at the spinous and granular layers (Fig. 3c). The transition between honeycomb and cobblestone patterns was often notable and demarcated the margins of the wound cavity at the level of the epidermis (Fig. 3d).

Bright adnexal structures were seen in only two lesions (5%). These were round structures in the dermis composed of uniformly spaced bright nuclei of adnexal epithelium.

Bright linear or curved structures were seen in the dermis in 25 (64%) lesions. The bright structures were found in a retiform arrangement or in parallel (bundles). These structures correlated with dermal collagen. In some cases, these linear structures were apparent in the background of amorphous brightness (Fig. 3e), which correlated with solar elastosis (Fig. 3f). Bright stellate cells and small bright dots in the dermis were seen in 25 (64%) lesions (Fig. 3g), correlating with inflammatory cells (histiocytes and lymphocytes, Fig. 3h).

#### Evaluation of shave biopsy wound margins with reflectance confocal microscopy

Evaluating the RCM mosaics of the surgical wounds, we identified three margin levels:

1 Epidermal margin – mosaics acquired at the level of surrounding epidermis (Fig. 4a, b). The central portion of the wound cavity appeared dark. Peripheral to it, bright nuclei forming a cobblestone pattern were seen; these were compatible with nuclei of epidermal keratinocytes in the outer, most superficial perimeter of the wound cavity. Peripheral to the wound, the epidermis in the surrounding skin showed a honeycomb pattern (Fig. 3d).

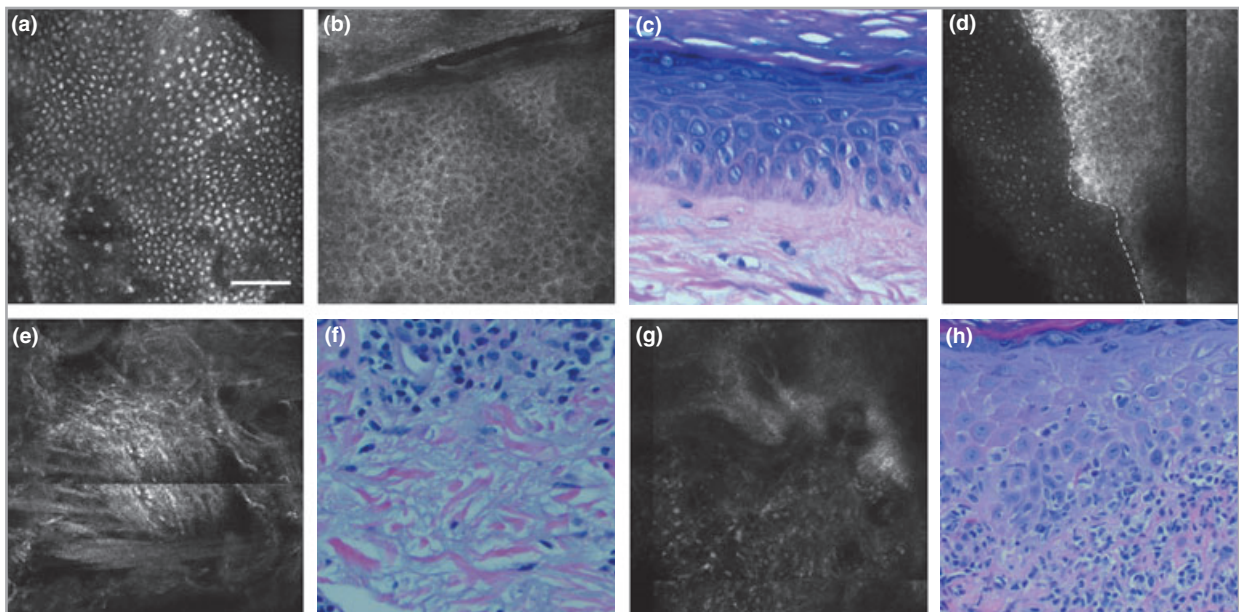


**Fig 3.** Histopathological correlation of reflectance confocal microscopy (RCM) features seen at shave biopsy margins. (a) Nuclei of keratinocytes that line the wound cavity appear bright, following application of aluminium chloride; this is referred to as cobblestone pattern. (b) Normal keratinocytes in the surrounding epidermis adjacent to the wound cavity display a different pattern, referred to as honeycomb pattern, whereby the nuclei are dark and the cellular outlines of keratinocytes are bright; (c) both patterns correlate with spinous and granular layers without atypia of keratinocytes. (d) Honeycomb pattern adjacent to cobblestone pattern; the dashed line of demarcation indicates the edge of the wound at the level of the epidermal margin. (e) Bright linear and curved structures in the dermis with a background of amorphous brightness seen on RCM correlated with collagen bundles in solar-altered dermis on histopathology (f). (g) Small round bright features and bright stellate cells in the dermis seen on RCM correlated with an infiltrate of lymphocytes and histiocytes on histopathology (h). Scale bar = 100  $\mu\text{m}$  on RCM images.

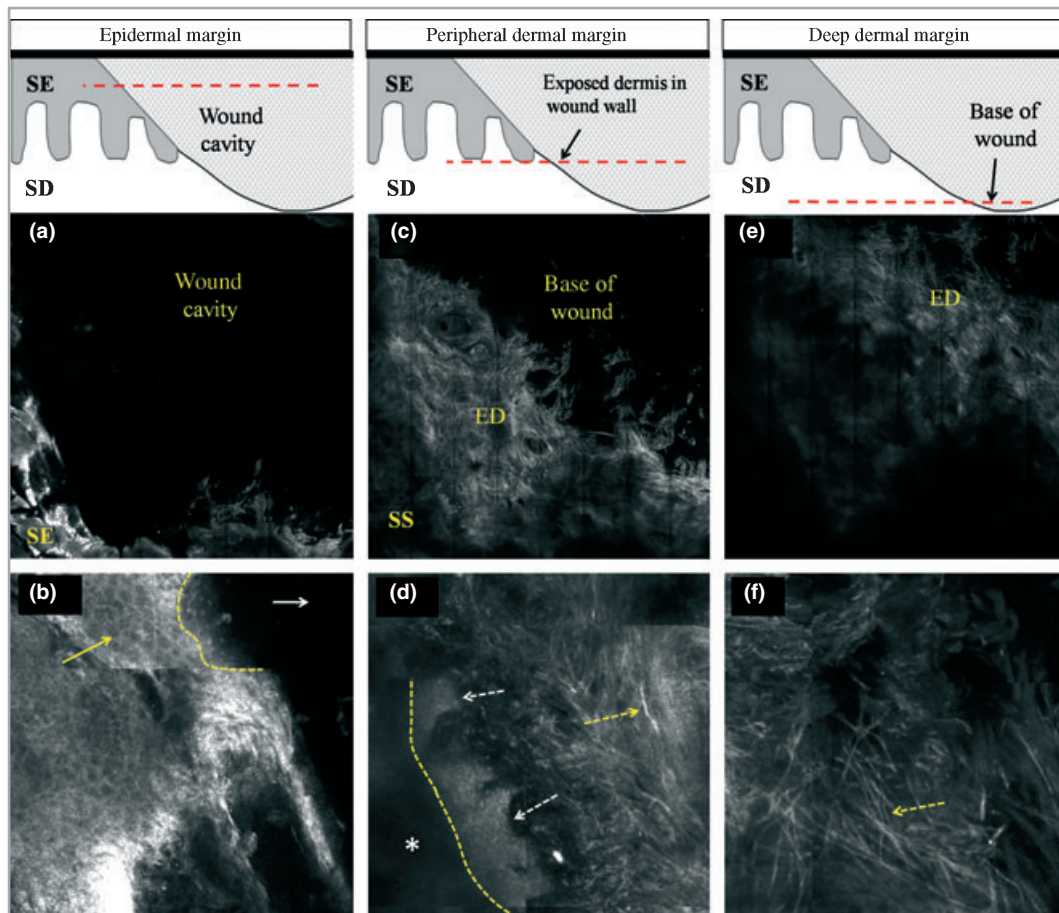


**Fig 4.** Wound margins at varying depths. The level of imaging is depicted by the dashed line in the drawings at the top of each column. SD, surrounding dermis. (a, b) Epidermal margin; the reflectance confocal microscopy (RCM) mosaic (a,  $4 \times 4$  mm) is taken at the level of the spinous layer of the epidermis. The surrounding epidermis (SE) displays a honeycomb pattern. The dark area represents the gel-filled wound cavity. At higher magnification RCM (b,  $0.5 \times 0.5$  mm) a regular honeycomb pattern in the surrounding epidermis (yellow arrow) can be seen, as well as a few bright nuclei in cobblestone pattern within the wound cavity (white arrow). The demarcation between honeycomb and cobblestone patterns, denoting the wound edge, is shown (yellow dashed line). (c, d) Peripheral dermal margin; in this RCM mosaic (c,  $4 \times 4$  mm) the surrounding skin (SS) is blurred as imaging is performed through intact stratum corneum, resulting in loss of backscattered detected light with increasing depth. In contrast, the exposed dermis (ED) in the wound shows bright reticulated collagen of the papillary dermis. The base of the wound is still below the plane of imaging and therefore appears dark. At higher magnification RCM (d,  $0.5 \times 0.5$  mm), there is demarcation (dashed yellow line) between the blurred surrounding skin (asterisk) and the exposed wound tissue showing bright dermal-epidermal junction (white dashed arrows) as well as bright, in-focus collagen in the superficial dermis (dashed yellow arrow). (e, f) Deep dermal margin; on RCM mosaic (e,  $4 \times 4$  mm) the surrounding dermis appears blurred and dark because of deeper imaging level. However, the RCM focal plane reaches the exposed dermis (ED) at the base of the wound, which appears bright. At higher magnification RCM (f,  $0.5 \times 0.5$  mm) the bright collagen bundles at the base of the wound can be seen (dashed yellow arrow).

2 Peripheral dermal margin – mosaics acquired at the level of the superficial dermis (Fig. 4c, d). The centre of the wound still appeared dark. Around it, within the wound cavity area, a bright area of tissue was seen. Depending on the level of the mosaic, this bright tissue area displayed either a cobblestone pattern of bright nuclei of keratinocytes (in the more superficial mosaics), or refractile structures in retiform or parallel arrangement (in the deeper mosaics) compatible with dermal collagen. Peripheral to the bright area, the surrounding dermis appeared less refractile, showing either dermal papillae of the dermal-epidermal junction or dermal collagen of the papillary dermis. Collagen in the surrounding dermis appeared more

blurred and less refractile than that within the exposed wound area. In addition, in some cases, with progressive imaging depth from the level of peripheral dermal margin to that of deep dermal margin, mosaics showed only a bright strip of wound margin at the focal plane of imaging. Central to this bright strip was the dark wound cavity, and peripheral to the bright strip the surrounding skin appeared minimally refractile to nonrefractile due to the imaging depth.

3 Deep dermal margin – mosaics acquired at the level of the base of the wound (Fig. 4e, f). The wound cavity that appeared dark at the level of the peripheral dermal margin now appeared bright, showing mostly highly refractile colla-

gen bundles. The surrounding skin and superficial edges of the wound appeared dark.

For mosaics with acceptable imaging quality, epidermal margin was visible in 23 of 39 lesions (59%), peripheral dermal margin was visible in 23 lesions (59%), and deep dermal margin was visible in 23 lesions (59%). All three margins were visible in 13 lesions (33%). Reasons for unacceptable quality of mosaic images included air bubbles obscuring images, oversaturation of image brightness compromising resolution, and inaccurate software stitching of images in the mosaic.

#### Correlation of confocal and histopathological features of skin neoplasms

In four lesions (10%), bright tumour islands were seen at deep dermal margins ( $n = 1$ ) and peripheral dermal margins ( $n = 3$ ). When tumour islands were observed in exposed wound margins, they were composed of bright closely aggre-

gated nuclei (Figs 5a, c and 6d). When tumour islands were located deeper in tissue, under the exposed surface or in the surrounding dermis, they appeared less refractile and individual nuclei were not discernible (Fig. 6e). Tumour islands correlated on histopathology with aggregates of basaloid cells showing peripheral palisading of nuclei (Figs 5b, d and 6f). In the surrounding dermis, a stroma composed of bright collagen bundles and bright stellate cells and small bright dots was observed (Fig. 6d); these bright cells correlated on histopathology with histiocytes and lymphocytes, respectively (Fig. 6f). In these four cases, histopathological diagnosis proved to be BCC, nodular in two lesions and superficial in two lesions.

In three lesions (8%), atypical honeycomb was observed in epidermal margins (Fig. 7g); histopathological diagnosis proved to be SCC. In one SCC lesion an atypical cobblestone pattern was seen in peripheral and deep dermal margins (Fig. 7e, f); this atypical cobblestone pattern displayed

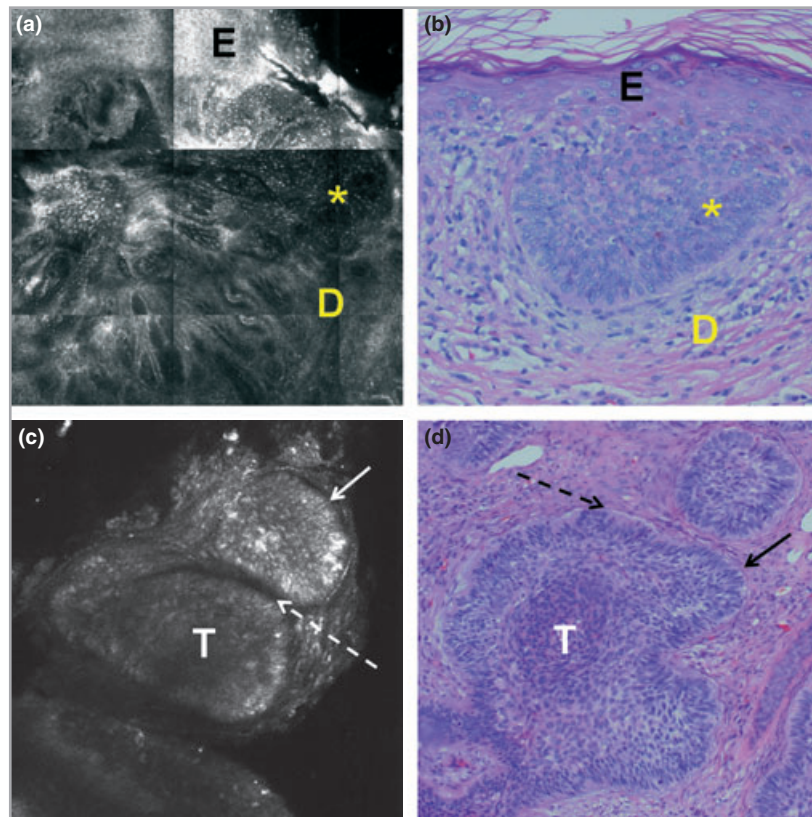


**Fig 5.** Basal cell carcinoma (BCC). Images a and b are from one lesion, images c and d from another lesion. (a) Reflectance confocal microscopy (RCM) imaging at the level of the dermal–epidermal junction (peripheral dermal margin) shows an aggregate of neoplastic cells appearing as a focus of bright nuclei (asterisk), well delineated from the adjacent epidermis (E) and dermis (D). (b) On histopathology an aggregate of basaloid cells with peripheral palisading of nuclei (asterisk) is emanating from the undersurface of the epidermis (E) and protruding into the superficial dermis (D). The diagnosis is superficial BCC. (c) RCM imaging at the level of the dermis (deep dermal margin) shows a dermal aggregate of neoplastic cells (T) displaying focal peripheral palisading of nuclei (solid arrow); the aggregates are well demarcated from the surrounding dermis by dark clefts (dashed arrow). (d) On histopathology, an aggregate of basaloid cells (T) is seen in the reticular dermis with palisading of nuclei (solid arrow) and subtle clefting (dashed arrow), diagnostic of nodular BCC. Notably, the tumours were transected during biopsy and appear at the exposed wound surface. As the neoplastic epithelial cells have been exposed to aluminium chloride application, the nuclei appear bright and help to delineate the tumour aggregates in RCM images.

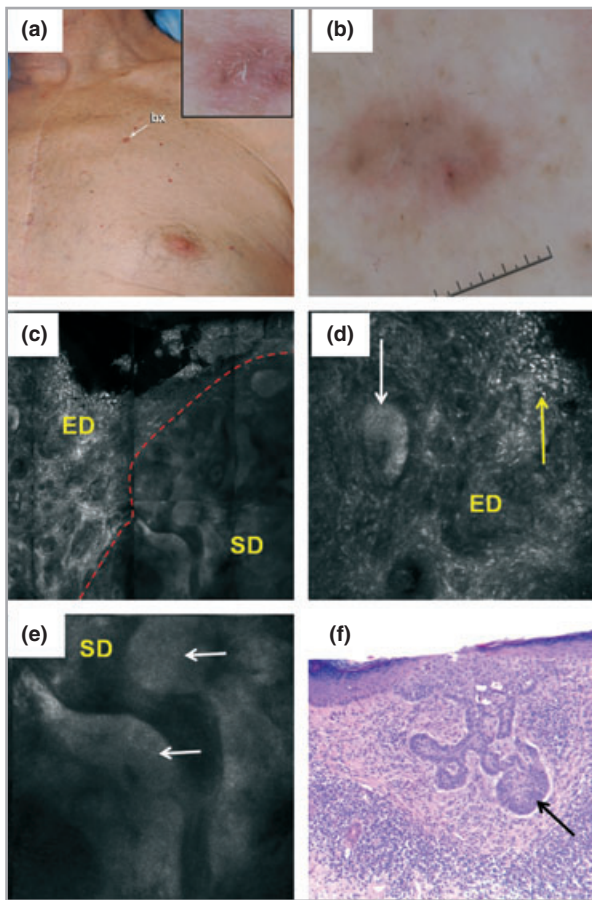


**Fig 6.** Basal cell carcinoma (BCC). (a) This patient presented an 8 mm papule on the chest (bx; inset shows close-up clinical image); (b) dermoscopy revealed grey dots and grey-brown ovoid nests, suspicious for BCC. (c) Reflectance confocal microscopy (RCM) mosaic ( $1.5 \times 1.5$  mm) of the shave biopsy wound is shown at the peripheral dermal margin level; the red dashed line demarcates the darker surrounding dermis (SD) from the brighter exposed dermis (ED). (d) Individual RCM image ( $500 \times 500 \mu\text{m}$ ) at the same level showing a bright tumour aggregate (white arrow) in the exposed dermis (ED) that also displays numerous bright spots and bright stellate cells (yellow arrow). (e) Individual RCM image ( $500 \times 500 \mu\text{m}$ ) in the surrounding dermis (SD) at the same level also showing tumour aggregates (white arrows). Note that these tumour aggregates and the surrounding dermis (e) appear less bright and with lower resolution than in the exposed dermis (d). (f) On histopathology, an aggregate of basaloid cells with peripheral palisading of nuclei (arrow) is emanating from the undersurface of the epidermis, diagnostic of superficial BCC. Note the dense inflammatory infiltrate which correlates with the numerous bright spots and bright stellate cells seen on RCM.

crowding of nuclei, variability in size and brightness of nuclei and the presence of abnormally large nuclei (Fig. 7h). On histopathology, crowding and pleomorphism of nuclei, hyperchromatic nuclei and disordered maturation of the epidermis were seen; the proliferation of atypical keratinocytes extended to the base and peripheral margins of the biopsy (Fig. 7i). Of note, in another case, while an atypical honey-

comb was observed in epidermal margins, the histopathological diagnosis proved to be lichen planus-like keratosis; in this case, mild atypia of keratinocytes, interpreted to be reactive to the lichenoid inflammation, was observed on histopathology.

## Discussion

One potential application of RCM is intraoperative imaging to assess cancer margins. We showed recently that BCC can be detected *ex vivo* in tissue excised during MMS.<sup>8,9</sup> Intraoperative margin mapping can further expedite MMS by obviating the need to wait for frozen pathology before proceeding with further surgery. However, RCM imaging of surgical wounds is challenging. *In vivo* RCM imaging is normally performed on intact skin which presents a flat surface, while intraoperative mapping requires imaging of crater-shaped wounds. Development of an RCM protocol for imaging contoured surfaces and use of RCM mosaics to evaluate wound margins has not been previously described.

$\text{AlCl}_3$  was used to improve visibility of tumours under RCM, as it was previously shown to enhance nuclear contrast.<sup>6</sup> We found that 20%  $\text{AlCl}_3$ , previously used by Tannous *et al.*,<sup>6</sup> requires a longer immersion time of 3 min; in comparison, 35%  $\text{AlCl}_3$  that is routinely used in our clinic requires only 1 min. While 50%  $\text{AlCl}_3$  achieved nuclear brightening even more rapidly, its use would require additional efficacy and safety study, as even lower concentrations of  $\text{AlCl}_3$  were shown to interfere with wound healing.<sup>31</sup> Previous studies showed that  $\text{AlCl}_3$  causes DNA to compact,<sup>32–34</sup> accounting for increased light backscatter of nuclei under RCM. This mechanism is similar to that observed with acetic acid ('aceto-whitening').<sup>35,36</sup>

Nuclear morphology of normal keratinocytes within the wound was enhanced by  $\text{AlCl}_3$ , producing a cobblestone pattern. The difference in nuclear morphology, being bright (cobblestone pattern) in exposed keratinocytes within the wound, and dark (honeycomb pattern) in keratinocytes in surrounding skin, allows for identification of epidermal wound margins. In addition, collagen bundles and inflammatory cells within the wound appeared much brighter than in surrounding dermis, allowing recognition of peripheral and deep dermal margins. Taken together, reproducible patterns were created by these bright tissue structures and were used as landmarks to identify RCM wound margin levels.

We showed feasibility of identifying residual neoplastic aggregates in shave biopsy wound margins. Nuclear brightening was seen in aggregates of BCC within the wound cavity; the RCM pattern of tumour islands was closely correlated with histopathological findings. Similarly, the nuclear enhancement of atypical keratinocytes in SCC allowed assessment of cellular criteria similar to those used in histopathology, such as nuclear crowding and pleomorphism of size. Of note, the effects of  $\text{AlCl}_3$  were limited to the wound cavity; in surrounding skin, brightening of nuclei was not seen and residual tumours were recognized only by using previously

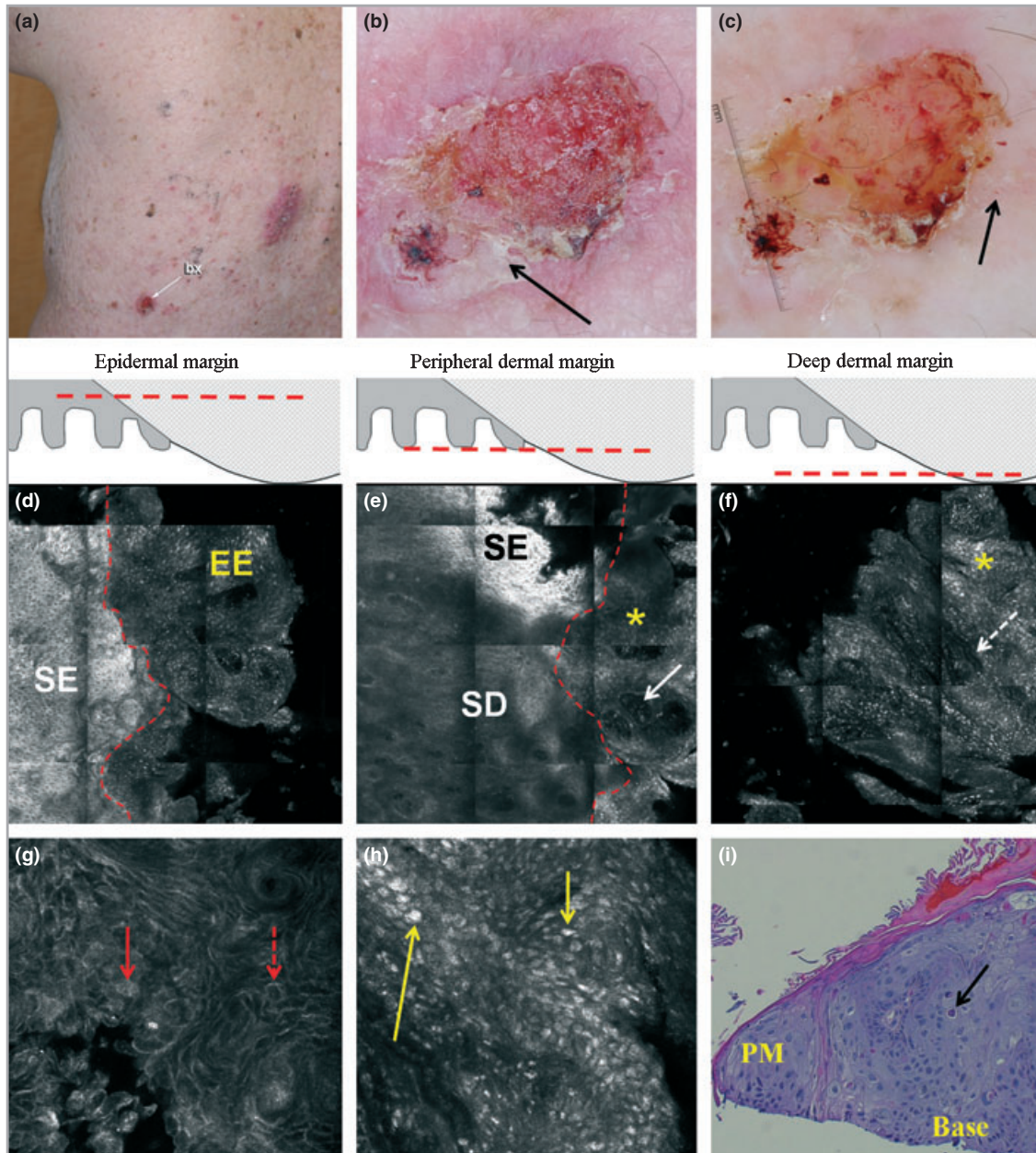


**Fig 7.** Squamous cell carcinoma (SCC). (a) This patient presented with a 1.5 cm red, keratotic plaque on the back (bx). (b) A close-up clinical image following shave biopsy showing the remaining scale in the surrounding skin (arrow). (c) Dermoscopy showing a pink blush and dotted vessels (arrow) in the skin surrounding the shave biopsy wound. (d) Reflectance confocal microscopy (RCM) mosaic (1.5 × 1.5 mm) at the level of epidermal margin (level indicated in the drawing above) showing a honeycomb pattern in the surrounding epidermis (SE), to the left of the dashed line. Note the enhanced brightness of nuclei in the exposed epidermis (EE, right of dashed line) producing a cobblestone pattern. (e) RCM mosaic (1.5 × 1.5 mm) at the level of peripheral dermal margin (level indicated in the drawing above). Both surrounding dermis (SD) and surrounding epidermis (SE) are seen to the left of the dashed line, indicating imaging is at the level of the dermal–epidermal junction. In the wound cavity, a cobblestone pattern is seen (asterisk) as well as dermal papillae (arrow). (f) RCM mosaic (1.5 × 1.5 mm) at the level of deep dermal margin, base of the wound (level indicated in the drawing above). The finding of cobblestone pattern (asterisk) in the dermis, where blood vessels can be seen (dashed arrow), is clearly abnormal. (g) RCM individual image (500 × 500 μm), akin to higher magnification microscopy, of the surrounding skin at epidermal margin level shows an atypical honeycomb pattern, with outlines that vary in thickness and brightness and dark holes (dashed red arrow) that vary in size and shape. There are cells that appear wholly bright, without central dark nucleus (solid red arrow). (h) RCM individual image (500 × 500 μm) of the exposed epidermis at the epidermal margin level shows an atypical cobblestone pattern, with bright nuclei of keratinocytes (yellow arrows) that are irregularly crowded and display variability in the size of nuclei. (i) On histopathology, there is full-thickness atypia of keratinocytes with jumbling, crowding and pleomorphism of nuclei, hyperchromatic nuclei and dyskeratotic keratinocytes (black arrow), diagnostic of SCC. The proliferation of atypical keratinocytes extended to the peripheral margins (PM) and base of the biopsy ('Base').

described criteria for RCM diagnosis of BCC and SCC in intact skin (e.g. atypical honeycomb in SCC).

The present study also identified limitations of current RCM. The device is relatively bulky and imaging is slow. As 6 × 6 mm mosaics were acquired in approximately 90 s, the minimum time to image each lesion was about 5 min. The use of an adhesive tissue ring limits access to one edge of the wound and precludes surveying the entire perimeter. Re-attaching the ring would wrinkle the taut transparent dressing, introducing imaging artifacts. Only superficial wounds can be imaged to the base with current RCM. Wounds with steep walls yielded *en face* mosaics with a thin ring of bright contrast and dark, blank spaces at the centre and periphery; these lesions required more mosaics to assess margins and therefore prolonged imaging time. To become practical, imaging surgical wounds requires new instrumentation in the form of a flexible hand-held probe and small objective lens, to enable full access and rapid imaging of the entire wound margin. Future software developments may include dynamic mosaicing algorithms that only image wound margins with bright contrast, where the mosaic provides diagnostic information, and avoids imaging blank spaces, reducing imaging time. Additionally, acceptable mosaic images in all three margins were obtained in only one-third of cases. This reflects limitation of instrumentation, as well as the learning curve for using the wound imaging protocol. We anticipate that with improved instrumentation, the majority of lesions will be better assessed at all three wound margin levels. Finally, findings on *en face* RCM images of wound margins were compared with findings in vertically oriented permanent histopathological sections. This constitutes indirect correlation of tissue structures. Direct comparison of RCM and histopathological findings of surgical margins would constitute a necessary step towards the implementation of RCM in surgery. To this end, we plan in future research to perform a clinical study in the MMS setting that will involve direct one-to-one comparison of *en face* RCM images with *en face* histopathological sections.

In conclusion, RCM imaging of superficial surgical wounds is feasible. The application of AlCl<sub>3</sub> enhances nuclear contrast of normal keratinocytes, inflammatory cells and neoplastic cells of BCC and SCC. The anatomical level of wound margins can be consistently identified in RCM mosaics. Conceivably, with advances in instrumentation and rigorous demonstration of sensitivity and specificity in clinical trials, RCM imaging may serve as a routine tool to evaluate cancer margins during surgery in the skin and other tissues.

### What's already known about this topic?

- Previous research showed that skin cancer can be diagnosed preoperatively with *in vivo* reflectance confocal microscopy (RCM) of intact skin, and intraoperatively with *ex vivo* RCM of excised tissue.

### What does this study add?

- We show feasibility of intraoperative, *in vivo* confocal imaging of shave biopsy wounds using aluminium chloride as contrast agent.
- We developed an imaging protocol for concave wounds, characterized wound margins by confocal landmarks, and detected residual skin cancer in wound margins.

### Acknowledgments

We thank Dr Allan Halpern and Dr Stephen Dusza for help in designing the study protocol, Dr Ashfaq Marghoob for help with accrual of patients, and the staff at Lucid Inc. (Dr Jay Eastman, Christi Alessi-Fox, William Fox and Zachary Eastman) for technical support.

### References

- 1 Bialy TL, Whalen J, Veledar E et al. Mohs micrographic surgery vs traditional surgical excision: a cost comparison analysis. *Arch Dermatol* 2004; **140**:736–42.
- 2 Rogers HW, Weinstock MA, Harris AR et al. Incidence estimate of nonmelanoma skin cancer in the United States, 2006. *Arch Dermatol* 2010; **146**:283–7.
- 3 Rajadhyaksha M, Grossman M, Esterowitz D et al. *In vivo* confocal scanning laser microscopy of human skin: melanin provides strong contrast. *J Invest Dermatol* 1995; **104**:946–52.
- 4 Rajadhyaksha M, González S, Zavislan JM et al. *In vivo* confocal scanning laser microscopy of human skin II: advances in instrumentation and comparison with histology. *J Invest Dermatol* 1999; **113**:293–303.
- 5 Nori S, Rius-Díaz F, Cuevas J et al. Sensitivity and specificity of reflectance-mode confocal microscopy for *in vivo* diagnosis of basal cell carcinoma: a multicenter study. *J Am Acad Dermatol* 2004; **51**: 923–30.
- 6 Tannous Z, Torres A, González S. *In vivo* real-time confocal reflectance microscopy: a noninvasive guide for Mohs micrographic surgery facilitated by aluminum chloride, an excellent contrast enhancer. *Dermatol Surg* 2003; **29**:839–46.
- 7 Al-Arashi MY, Salomatina E, Yaroslavsky AN. Multimodal confocal microscopy for diagnosing nonmelanoma skin cancers. *Lasers Surg Med* 2007; **39**:696–705.
- 8 Karen JK, Gareau DS, Dusza SW et al. Detection of basal cell carcinomas in Mohs excisions with fluorescence confocal mosaicing microscopy. *Br J Dermatol* 2009; **160**:1242–50.
- 9 Gareau DS, Karen JK, Dusza SW et al. Sensitivity and specificity for detecting basal cell carcinomas in Mohs excisions with confocal fluorescence mosaicing microscopy. *J Biomed Opt* 2009; **14**:034012.
- 10 Makhlof H, Gmitro AF, Tanbakuchi AA et al. Multispectral confocal microendoscope for *in vivo* and *in situ* imaging. *J Biomed Opt* 2008; **13**:044016.
- 11 Udovich JA, Besselsen DG, Gmitro AF. Assessment of acridine orange and SYTO 16 for *in vivo* imaging of the peritoneal tissues in mice. *J Microsc* 2009; **234**:124–9.
- 12 Ahlgrimm-Siess V, Massone C, Scope A et al. Reflectance confocal microscopy of facial lentigo maligna and lentigo maligna melanoma: a preliminary study. *Br J Dermatol* 2009; **161**:1307–16.

- 13 Rishpon A, Kim N, Scope A *et al.* Reflectance confocal microscopy criteria for squamous cell carcinomas and actinic keratoses. *Arch Dermatol* 2009; **145**:766–72.
- 14 Braga JC, Scope A, Klaz I *et al.* The significance of reflectance confocal microscopy in the assessment of solitary pink skin lesions. *J Am Acad Dermatol* 2009; **61**:230–41.
- 15 Hofmann-Wellenhof R, Wurm EM, Ahlgrimm-Siess V *et al.* Reflectance confocal microscopy – state-of-art and research overview. *Semin Cutan Med Surg* 2009; **28**:172–9.
- 16 Rajadhyaksha M. Confocal microscopy of skin cancers: translational advances toward clinical utility. *Conf Proc IEEE Eng Med Biol Soc* 2009; **2009**:3231–3.
- 17 Terushkin V, Wang SQ. Mohs surgery of basal cell carcinoma assisted by dermoscopy: report of two cases. *Dermatol Surg* 2009; **35**:2031–5.
- 18 Stenquist B, Ericson MB, Strandeberg C *et al.* Bispectral fluorescence imaging of aggressive basal cell carcinoma combined with histopathological mapping: a preliminary study indicating a possible adjunct to Mohs micrographic surgery. *Br J Dermatol* 2006; **154**:305–9.
- 19 Redondo P, Marquina M, Pretel M *et al.* Methyl-ALA-induced fluorescence in photodynamic diagnosis of basal cell carcinoma prior to Mohs micrographic surgery. *Arch Dermatol* 2008; **144**:115–17.
- 20 Alkalay R, Alcalay J, Maly A *et al.* Fluorescence imaging for the demarcation of basal cell carcinoma tumor borders. *J Drugs Dermatol* 2008; **7**:1033–7.
- 21 Bobadilla F, Wortsman X, Muñoz C *et al.* Pre-surgical high resolution ultrasound of facial basal cell carcinoma: correlation with histology. *Cancer Imaging* 2008; **8**:163–72.
- 22 Marmur ES, Berkowitz EZ, Fuchs BS *et al.* Use of high-frequency, high-resolution ultrasound before Mohs surgery. *Dermatol Surg* 2010; **36**:841–7.
- 23 Mogensen M, Joergensen TM, Nürnberg BM *et al.* Assessment of optical coherence tomography imaging in the diagnosis of non-melanoma skin cancer and benign lesions versus normal skin: observer-blinded evaluation by dermatologists and pathologists. *Dermatol Surg* 2009; **35**:965–72.
- 24 Larraona-Puy M, Ghita A, Zoladek A *et al.* Development of Raman microspectroscopy for automated detection and imaging of basal cell carcinoma. *J Biomed Opt* 2009; **14**:054031.
- 25 Lieber CA, Majumder SK, Ellis DL *et al.* In vivo nonmelanoma skin cancer diagnosis using Raman microspectroscopy. *Lasers Surg Med* 2008; **40**:461–7.
- 26 Gareau DS, Patel YG, Li Y *et al.* Confocal mosaicing microscopy in skin excisions: a demonstration of rapid surgical pathology. *J Microsc* 2009; **233**:149–59.
- 27 Gareau DS, Li Y, Huang B *et al.* Confocal mosaicing microscopy in Mohs skin excisions: feasibility of rapid surgical pathology. *J Biomed Opt* 2008; **13**:054001.
- 28 Patel YG, Nehal KS, Aranda I *et al.* Confocal reflectance mosaicing of basal cell carcinomas in Mohs surgical skin excisions. *J Biomed Opt* 2007; **12**:034027.
- 29 Gareau DS, Patel YG, Rajadhyaksha M. Basic principles of reflectance confocal microscopy. In: *Reflectance Confocal Microscopy of Cutaneous Tumours* (González S, Gill M, Halpern AC, eds). London: Informa Healthcare, 2008; 1–6.
- 30 Scope A, Benvenuto-Andrade C, Agero AL *et al.* In vivo reflectance confocal microscopy imaging of melanocytic skin lesions: consensus terminology glossary and illustrative images. *J Am Acad Dermatol* 2007; **57**:644–58.
- 31 Sawchuk WS, Friedman KJ, Manning T, Pinnell SR. Delayed healing in full-thickness wounds treated with aluminum chloride solution. A histologic study with evaporimetry correlation. *J Am Acad Dermatol* 1986; **15**:982–9.
- 32 Karlik SJ, Eichhorn GL, Lewis PN, Crapper DR. Interaction of aluminum species with deoxyribonucleic acid. *Biochemistry* 1980; **19**:5991–8.
- 33 Karlik SJ, Eichhorn GL. Polynucleotide cross-linking by aluminum. *J Inorg Biochem* 1989; **37**:259–69.
- 34 Matsuzawa Y, Kanbe T, Yoshikawa K. Compaction and multiple chain assembly of DNA with the cationic polymer poly(aluminum chloride) (PAC). *Langmuir* 2004; **20**:6439–42.
- 35 Drezek RA, Collier T, Brookner CK *et al.* Laser scanning confocal microscopy of cervical tissue before and after application of acetic acid. *Am J Obstet Gynecol* 2000; **182**:1135–9.
- 36 Rajadhyaksha M, González S, Zavislan JM. Detectability of contrast agents for confocal reflectance imaging of skin and microcirculation. *J Biomed Opt* 2004; **9**:323–31.